

Model generation of viral channel forming 2B protein bundles from polio and coxsackie viruses

GEORGE PATARGIAS¹, THOMAS BARKE¹, ANTHONY WATTS¹, & WOLFGANG B. FISCHER^{1,2}

¹Biomembrane Structure Unit, Department of Biochemistry, Oxford University and ²Bionanotechnology Interdisciplinary Research Centre, Clarendon Laboratory, Department of Physics, Oxford University, Oxford, UK

(Received 20 March 2009; and in revised form 22 June 2009)

Abstract

2B is a 99 amino acid membrane protein encoded by enteroviruses such as polio and coxsackie viruses with two transmembrane domains. The protein is found to make membranes of infected cells permeable. Using a computational approach which positions the models and assesses stability by molecular dynamics (MD) simulations a putative tetrameric bundle model of 2B is generated. The bundles show a pore lining motif of three lysines followed by a serine. The bundle is discussed in terms of different possible orientations of the helices in the membrane and the consequences this has on the *in vivo* activity of 2B.

Keywords: 2B, polio virus, coxsackie virus, membrane proteins, assembly, channels

Introduction

Viral channel and pore forming proteins, also called viroporins [1], induce a change of the permeability of host cell membranes thereby improving the mode of action of the virus within the host cell [2,3]. In many cases the amino acid sequence of the putative channel forming proteins are known, but their role, mechanism of function and structure still remains to be elucidated.

Computational methods are a valuable tool modelling structural and eventually also mechanistic features of a protein. With the lack of structural information these methods rely on assumptions which need to be made to generate a potential '*in vivo*' protein structure. One of the assumptions is that the proteins, produced in the ER, follow the so called two-stage model of membrane protein folding and oligomerization which has been recently expanded into the three stage model [4–6]. More steps need to be elucidated when constructing finally an ion or substrate conducting pore. The two-stage model holds for the oligomerization of helical transmembrane domains (TMDs) when dealing with polytopic proteins such as 2B from Polio virus [7–9] and p7 from HCV [10,11], each having two TMDs, and 3a from SARS-CoV with three TMDs [12].

Experimental data of the number of monomers forming the assembly are difficult to obtain. Computational methods may serve to deliver this information until further experimental data are available. Several approaches have already been described and used in the literature [13–20].

In this study, a protocol is employed which enable the generation of assemblies of two or more helices which are seen as the 'monomeric subunit' of larger bundles or pores (see also [21,22]). The protocol builds on a fast generation of helices, generation of monomers (monomeric subunits) out of the individual helices and finally copies of the monomers around a central axis forming the model pore. After each of the steps the models are equilibrated with multi nano second molecular dynamics (MD) simulation.

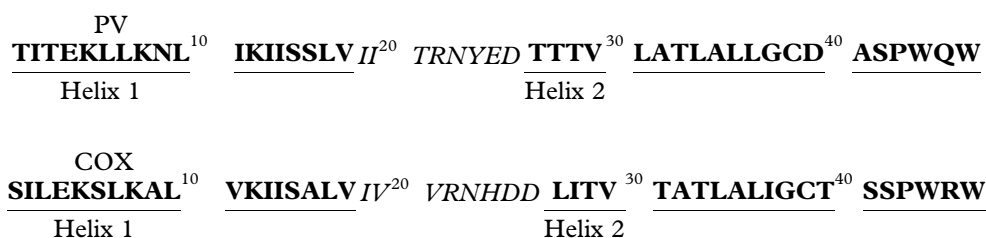
2B from Polio virus has been chosen to study fast assembly protocols. 2B is a 99 amino acid non-structural protein encoded also by other enteroviruses such as coxsackie and ECHO viruses [23,24]. The protein is mostly located in the Golgi and endoplasmic reticulum where it is involved in change of Ca²⁺ concentration in the stores [25]. 2B is assumed to consist of two TMDs which oligomerize and form SDS-PAGE resistant tetramers

Correspondence: Wolfgang B. Fischer, currently at Institute of Biophotonics, Department of Medical Science and Engineering, National Yang-Ming University, Taipei, Taiwan. Tel: +886 2 2826 7394. Fax: +886 2 2823 5460. E-mail: wfischer@ym.edu.tw

[7,9,26–29]. One of the TMDs is amphipathic (helix 1) and mutations of the positive charges (lysines) in this region abrogate viral growth [30], the other (helix 2) is more hydrophobic. Permeability studies have shown a defined cut-off size for the permeating substrates to be in the order of 660 kDa indicating a possible topological flexibility. Structural information is lacking to date.

Materials and methods

The following sequences were taken to model the two transmembrane (TM) helices of 2B from Polio virus (PV used to indicate the structural models) and coxsackie virus (COX):



The amino acids used to model the TMDs are underlined and shown in bold. The residues in italics indicate the linker region between the two TMDs.

Generation of single helices

Single helices were generated using X-PLOR [31] and a simulated annealing (SA) protocol combined with MD simulations. The SA/MD protocol has been used in previous work [11,17] where it is explained in detail. The protocol consists of two stages. In a first stage an ideal α -helix based on the $C\alpha$ atoms was generated with 5° initial tilt. The side chain atoms were superimposed onto the $C\alpha$ atoms. Gradually the side chain atoms were produced during an annealing phase starting at 1000 K, with weight factors increasing for bond length, bond angle planarity and chirality. After an initial delay a repulsive van der Waals (vdW) term was introduced and the helix cooled to 300 K in steps of 10 K/0.5 ps with the van der Waals radii reduced to 80% of their original values. This allowed the atoms to pass each other and to avoid any inaccurate conformation. Repeating this procedure five times delivered five structures. Each of these structures was then used five times in a short MD simulation (stage 2) with initial velocities corresponding to 500 K. The $C\alpha$

atoms were able to move freely within their particular topology when the temperature was decreased from 500–300 K. At this stage the partial charges (PARAM19) were introduced, gradually scaled up from 0.005–0.4 of their full value and kept at this value for the rest of the protocol. At 300 K a 5 ps MD simulations (CHARMM force field, Verlet integration method) was performed followed by a 1000 step conjugate gradient minimization. A distance-dependent dielectric function was used with a switching function smoothly truncating the long-range electrostatic interactions. Out of the 25 structures generated in stage 2 one structure was chosen, which was not seen with any kink. The structure was embedded in a fully solvated 128

POPC (1-palmitoyl-2-oleoyl-*sn*-glycerol-3-phosphatidylcholine) lipid bilayer and subjected to 800 ps equilibration run followed by 3 ns of MD simulation.

Generation of 2B monomers

All calculations were performed using the Crystallography and NMR System (CNS) [32] with the OPLS parameter set and united atom topology, explicitly describing only polar and aromatic hydrogens. The 2B monomers were generated from pairs of ideal helices generated as mentioned above.

The conformations of the TM helix pairs were searched starting from both left and right crossing angles (-25° or $+25^\circ$), with the helices rotating from 0 – 360° in 45° increments. Each of these pairs was subjected to four simulation runs of 200 steps, with a step size of 0.004 ps at 300 K. The resulting 512 structures were grouped into clusters. A cluster was defined as having at least 10 structures with a relative root-mean-square-deviation of the backbone atoms of not more than 1.0 Å from one member of the cluster to another member of the same cluster. The average structure of each cluster was used for further analysis (see values in Tables I and II). In the text, the term *cluster* refers to the average structure of a cluster of helical pairs.

Before running the MD simulations of the monomers in a fully hydrated lipid bilayer each of the helical pairs (monomers) was connected with the amino acids of the linker region. The ‘Loopy’ program within Jackal 1.5 package for modelling and analysis of protein structures was applied to place the amino acids [33]. The Loopy program uses the colony energy approach to account for entropic effects and fast torsion space minimizer to speed up the conformation sampling. The monomers were then inserted into a 128 molecule POPC bilayer. An 800ps equilibration was carried out (see Supplementary Figure, online version only) before the full 10 ns simulation.

Generation of tetramers

Tetramers were generated using an XPLOR script which duplicates, rotates and translates a monomer so as to create a tetramer with rotational symmetry about the centre. An orientation of the helix was chosen which positions the polar residues towards the center of the tetramer and the hydrophobic residues forming contacts with neighbouring monomers or the lipid tails of the bilayer. Such an orientation of the monomers has been assumed to stabilize bundle structure and has been supported by experimental evidence [29]. The orientation has also been chosen to form other bundles of viral channel forming proteins [11,34,35].

Tetramers were inserted into a larger, 288 molecule POPC bilayer. As with the single helices and monomers, an 800 ps equilibration simulation was carried out with protein movement restrained to allow the lipids to pack around the protein (see

Table I. Buried surface area (BSA) of the averaged structures of Polio and Coxsackie 2B monomers taken from the cluster calculations shown in Figure 2. The listed values were extracted from solvent accessible area calculations using the program Naccess [36].

Cluster no	Buried surface area (\AA^2)	
	Polio	Coxsackie
1	1114	1060
2	1280	1023
3	1172	1318
4	1160	1167
5	1007	1198
6	1246	1297
7	1214	1157
8	1256	1127
9	974	1154
10	1262	1030
11	1054	1085
12		1175
13		1100
14		1089

Supplementary Figure, online version only). In the case of the tetramers, the equilibration allowed water molecules to fill the pore. All tetramers were subject to an unrestrained simulation of 11 ns.

Molecular Dynamics simulations

All simulations were carried out with GROMACS 3.2.1 package. The simulations were conducted in the *NPT* ensemble employing Berendsen algorithm of coupling to an external bath of constant temperature of 300 K, and pressure of 1 bar in all directions. Protein, lipid, water atoms and ions were separately coupled to the external temperature bath and as a system to the pressure baths with coupling constants $\tau_T = 0.1$ ps and $\tau_p = 1.0$ ps, respectively. The ‘leap-frog’ reference algorithm was used for the numerical integration of the equations of motion with a time step of 2 femto seconds for an overall simulation time of *ca.* 1.2 ns. Energy minimizations were performed employing the steepest descent algorithm. The GROMOS96 force field was used as implemented in GROMACS. All bond distances in the system were constrained through the LINCS algorithm. The electrostatic interactions were computed using the Particle Mesh Ewald (PME) summation algorithm and vdW interactions were modelled using a 6-12 Lennard-Jones potential with a 1 nm cut-off. The total number of atoms for the single helix simulations was between 22953 and 24384, the 2B monomers between 22674 and 23169 and the tetramers between 36492 and 53237.

Naccess (www.bioinf.manchester.ac.uk/naccess/) was used to calculate the solvent accessible area (SAS) of the monomers. In this program a probe of given radius (typically 1.4 \AA) is rolled around the Van der Waals (vdW) surface of the molecule, and the path traced out by its centre is the solvent accessible surface [36]. The buried surface area (BSA) of a helical dimer was then determined by adding the SAS of the individual helices and subtracting this value from the SAS of the helical dimer.

Results

The single helices and monomers

The individual helices are placed in a fully hydrated lipid bilayer to derive an equilibrated structure. The root mean square deviation (RMSD) of the $C\alpha$ atoms for each of the individual helices level off after 0.5 ns and fluctuate around 0.1 nm (Figure 1A) indicating minor conformational changes compared to their initial starting structure. The values for helix 2 of PV protein rise to 0.3 nm after 1.5 (Figure 1A, grey dashed line). This rise is due to an increase in kink angle around Ala-32. The kink angle changes

Table II. Total, electrostatic and vdW energies of the averaged structures of the 2B monomers using CHI as part of the CNS software [32]. Structures were taken from cluster calculations shown in Figure 2. All values are given in kJ/mol.

Cluster no	Energy		Electrostatic		vdW	
	Polio	Coxsackie	Polio	Coxsackie	Polio	Coxsackie
1	-1674	-1510	-1815	-1694	53.4	76.1
2	-1575	-1491	-1716	-1657	43.1	62.5
3	-1725	-1483	-1867	-1655	57.8	51.0
4	-1717	-1388	-1847	-1638	36.9	57.7
5	-1648	-1487	-1804	-1666	67.0	71.7
6	-1588	-1483	-1723	-1700	56.6	62.6
7	-1618	-1515	-1764	-1672	43.4	58.4
8	-1745	-1576	-1913	-1736	62.2	67.1
9	-1708	-1502	-1864	-1655	68.9	62.0
10	-1615	-1448	-1752	-1671	46.4	75.8
11	-1679	-1511	-1817	-1687	54.4	74.6
12		-1468		-1636		59.0
13		-1510		-1730		66.1
14		-1376		-1656		74.1

from $\sim 20^\circ$ to $\sim 45^\circ$ during this time period (data not shown). The kink disappears later in the simulation and is not observed during the simulations of the monomers and tetramers.

The 2B monomers are selected using a minimum RMSD cut-off between structures of 1.0, and a cluster size of at least 10. These parameters lead to the generation of 11 PV clusters (Figure 2A) and 14 COX clusters (Figure 2B). Figure 2 contains all clusters and groups with the left handed structures in the left panel and the right handed structures in the right panel. Plotting the rotational angles of each of the two helices (ϕ_1 of helix 1 and ϕ_2 of helix 2) for each of the clusters shows that PV clusters 3 and 4 (Figure 2A, left panel) and COX clusters 6 and 8 (Figure 2B, left panel) have helices with the same rotation. Based on the ϕ angles clusters PV3 and COX6 adopt rotational angles of $\phi_1 \sim 30^\circ/\phi_2 \sim 120^\circ$. Structures of clusters PV4 and Cox 8 have values of $\phi_1 \sim 210^\circ/\phi_2 \sim 100^\circ$. All clusters adopt a left handed structure.

Even though PV cluster 3 (PV3; Figure 3A) has been identified to be similar to COX cluster 6 (COX6; Figure 3C) the buried surface areas of the two clusters are quite different (with PV3 having a value of 1172 \AA^2 and COX6 a value of 1297 \AA^2 [Table I]). Also the values for electrostatic interactions and total energy differ (Table 2). This suggests that different interactions occur between the helices. Both clusters have VdW energies of about 50–60 kJ/mol. All values are taken from the averaged structures, indicated as A of each of the cluster in Figure 2.

PV cluster 4 (PV4; Figure 3B) has been identified to be similar to COX cluster 8 (COX8; Figure 3D), even though PV4 shows a different value for the buried surface (1160 \AA^2 , PV4, and 1127 \AA^2 , COX8;

Table I). Whereas PV4 has the most favorable VdW interaction of all PV clusters (36.9 kJ/mol; Table II), the COX8 VdW energy is about 67 kJ/mol. The lowest, most favorable energy values (both total energy, -1576 kJ/mol , and electrostatic energy -1736 kJ/mol) out of the COX clusters is calculated for COX8.

Other clusters which show favorable interactions are COX3 and PV8. COX3 has the highest BSA (1318 \AA^2 , Table I) and best VdW energy (51 kJ/mol, Table II) out of the COX clusters, although its total energy is high (-1483 kJ/mol , Table II). PV8 also shows a high buried surface area of 1256 \AA^2 , as well as having the lowest total energy value (-1745 kJ/mol), but has non-favorable VdW interactions (62.2 kJ/mol).

PV3 and COX6 are chosen for simulations as they show similar orientations of their helices, suggesting the possibility that they could form tetramers with similar structures. PV3 also has the lowest energy (-1725 kJ/mol) besides PV8. COX6 has the second highest buried surface area (1297 \AA^2) and third best electrostatic energy (-1700 kJ/mol) out of the COX clusters. PV4 and COX8 are also chosen for simulation based on the same helix orientation. PV4 shows the lowest VdW energy (36.9 kJ/mol) out of the PV clusters and COX8 has the best total (-1576 kJ/mol) and electrostatic energy (-1736 kJ/mol) out of the COX clusters.

Considering both buried surface area and total energy does not give a consistent picture in terms of the ranking of the clusters. Ranking according to individual criteria (overlap, buried surface, VdW, electrostatics and total energy) shows that PV3 and COX8 appear to be amongst the top 3 for each individual criterion.

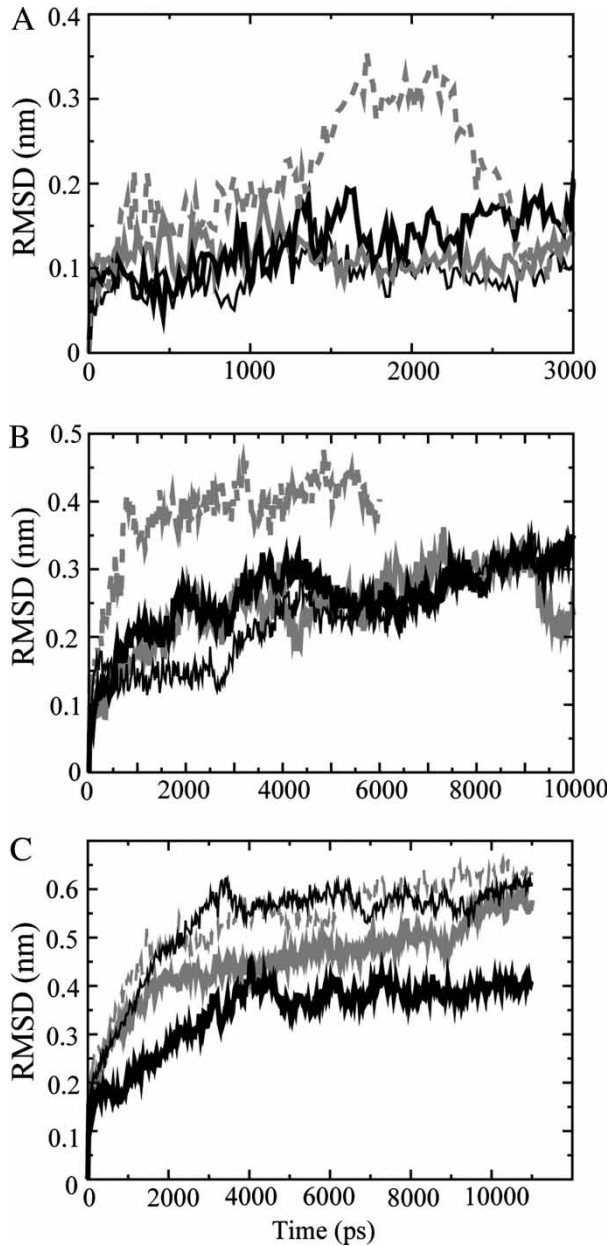


Figure 1. Root mean square deviation (RMSD) of the $C\alpha$ atoms for the single helices (A) with helices 1 from PV (thick black line) and COX (thin black line) and helices 2 for PV (grey dashed line) and COX (grey line), the 2B monomers (B) with PV4 (thick black line), PV3 (thin black line), COX8 (thick grey line) and COX6 (dashed grey line), and the respective tetrameric bundles (C).

For the successive modelling the averaged structure over all the members of the cluster is calculated and used.

All lysine residues, Lys-5, -8, and -12 of helix 1 in all simulations of the single helix (Figure 4A, PV4 as an example) and the 2B monomers interact with water and polar headgroups at either side of the bilayer surface.

Using the program 'Loopy', the two helices of the clusters are connected to form 2B monomers.

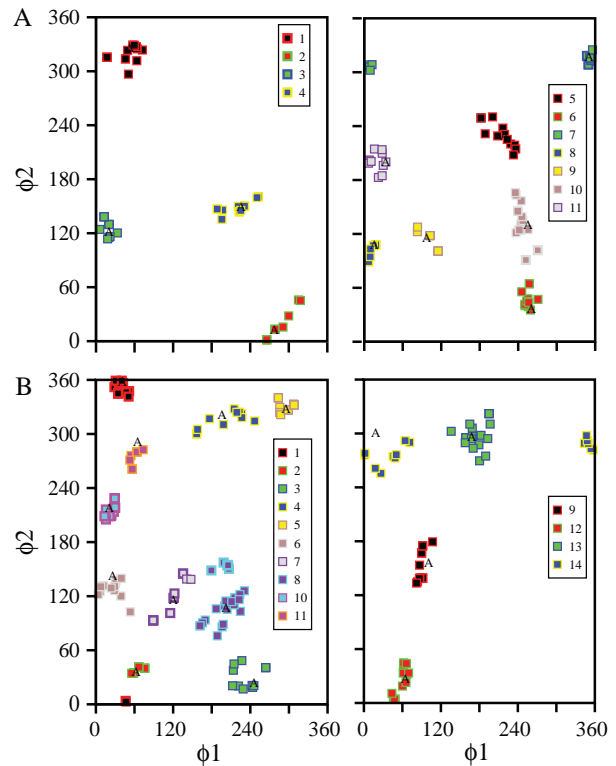


Figure 2. Monomer structures generated by CHI represented by their ϕ_1 and ϕ_2 values indicative for the handedness of the helical pairs. ϕ_1 represents the rotation of helix 1 relative to its starting position and ϕ_2 represents the rotation of helix 2. The data from PV are shown in the top row (A), those for the COX in the bottom row (B). For (A) and (B) the left handed structures are shown in the left panel and the right handed structures in the right panel. 'A' indicates the values for the averaged structure of each of the clusters.

RMSDs of each of these monomers simulated for 10 ns (6 ns in case of COX6) are shown in Figure 1B. Whilst COX8, PV3 and 4 are leveling off at around 0.25 nm, COX6 shows rather high RMSD values of around 0.4 nm. A visible inspection shows that the two helices are tilted in opposite directions to one another. Helix 1 adopts a tilt of 25° and helix 2 a tilt of -35° , causing less interactions between them.

The inter-helical loop contains a string of residues (Arg-Asn-Tyr-Glu in PV, Arg-Asn-His in COX) with non-zero amphiphilicity index [36] (except for Asn), suggesting a preference for being situated at the membrane-water interface. Figure 4B and 4D show PV4 with asparagine, arginine, tyrosine and glutamate residues (all in space filled mode) interacting at the lipid-water interface. Also the two tryptophans in helix 2 reside at the lipid-water interface (Figure 4B).

The conformation of the COX6 monomer after 6 ns was such that it would produce a tetrameric bundle structure with minimal interactions between helix 2 and other monomers (data not shown). This

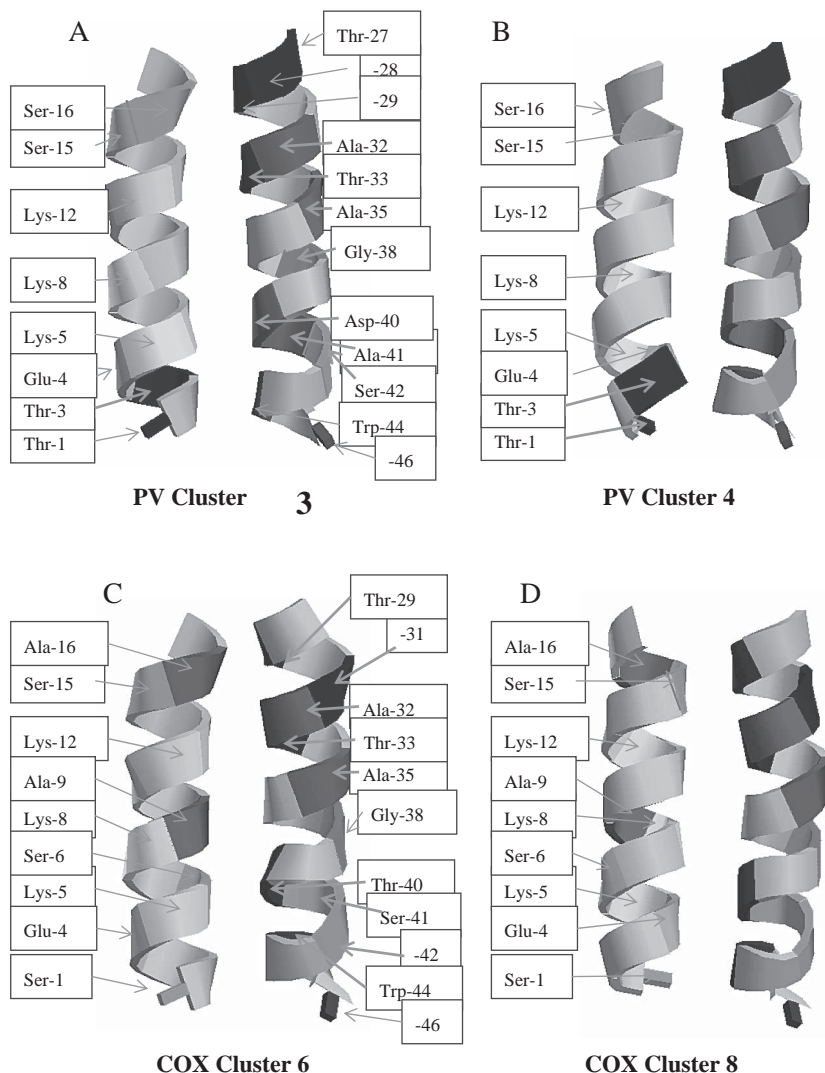


Figure 3. Averaged structures (indicated as A in Figure 2) of the 2B monomers of the PV3 (A), PV4 (B), COX6 (C) and COX8 (D) cluster. The individual residues are marked by an arrow, in addition a grey scale colour code according to RASMOL is used. For the sake of clarity, in (C) and (D) the second helix (right) has no labels. The labels are according to the second helix in (A) and (B). This figure is reproduced in colour in the online version.

structure would therefore not be in accord with the mutational data, which show that specific hydrophobic residues in helix 2 are essential for oligomerization [38]. It would therefore appear that a COX6 tetramer would not be stable due to poor interactions between the monomers.

Tetramer simulations

The RMSD values for all the four bundles rise to an approximate level between 0.3 and 0.6 nm within the first 3 ns and remain on their individual levels for the rest of the simulation (Figure 1C).

The bundles are modelled so that the hydrophilic residues of the amphipathic helix 1 point into the lumen of the pore (Figure 5A). After 11 ns simulation the PV4 tetramer the overall orientation of all

the residues remains so that the polar residues face the centre of the putative pore (Figure 5B). After 4 ns the narrowest point of the pore varies between 5 and 7 Å allowing for a continuous water column in the lumen of the pore (Figure 5C). Residues Lys-5, -8, -12 and Glu-25 are part of the hydrophilic lumen of the bundle (Figure 6A), so are Ser-16 and -15 (Figure 6B). Ala-32, -35 are located towards the helix1/-2 interface suggesting that it supports the packing (Figure 6C). Trp-44 also adopts a position which enables the residue to point into the pore (Figure 6C). The residues linking the two helices, Arg-22 and Glu-25, are in a position that may affect the electrostatics at the entrance of the channel lumen (Figure 7).

The averaged BSA over all the monomers of PV4 calculated at three different time points during the

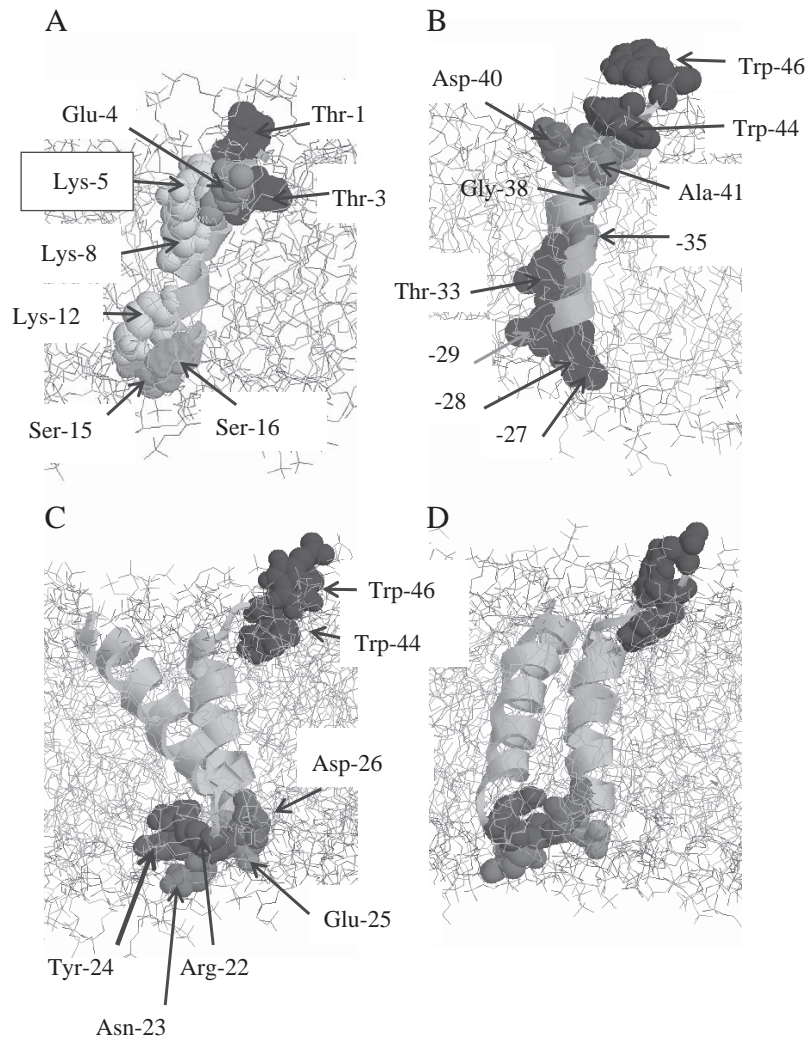


Figure 4. PV4 helix 1 (A) and helix 2 (B) shown with the relevant residues indicated by arrows. The residues are shown in vdW representation and highlighted using a grey scale colour code (RASMOL). The lipid membrane is shown in stick mode, water molecules are omitted for clarity. The monomers seen from different perspectives (C and D). The residues are indicated by arrows and are also highlighted in a grey scale colour representation. This figure is reproduced in colour in the online version.

MD simulation has decreased from $(669.6 \pm 37.9) \text{ \AA}^2$ (0 ns) to $(350.6 \pm 184.8) \text{ \AA}^2$ (5 ns) and $(302.4 \pm 190.6) \text{ \AA}^2$ (11 ns). During the same time lipid thickness remains unaffected with averaged values of $(34.4 \pm 0.2) \text{ nm}$ calculated from the first half of the simulation (taken from snapshots at 0, 2 and 4 ns) and $(33.7 \pm 0.1) \text{ nm}$ calculated from the last half of the simulation (taken from snapshots at 6, 8, 10 and 11 ns). The values BSA and lipid thickness calculated for the other bundles follow the same trend (data not shown). The initial decrease of BSA from 1160 \AA^2 to 669 \AA^2 is due to a loss of contact caused by the minimization features applied in the MD simulation protocol.

The data of the BSA indicate that during the simulation the monomer loses some of its closed packing. The time evolution of the data in combination with the RMSD results (PV4, thick black line,

Figure 4C) supports the assumption that the system reaches an equilibrated state under the applied experimental conditions.

The PV4, the PV3 tetramer appears to equilibrate after 4 ns with a pore diameter varying between 5 and 7 \AA (data not shown). However, there is a greater change from the starting structure of the protein. This is seen especially for one of the monomers, for which the amphipathic helix shows a tilt of 50° in respect to the bilayer. The major change in protein structure for the COX8 tetramer is an increase of the tilt angles of the amphipathic helices from 15° to about 40° (data not shown). A constriction is visible towards the end with the loops, which reduces the diameter to 3 \AA . With the widening towards the N- and C termini ($6\text{--}8 \text{ \AA}$) the tetrameric bundle adopts a tepee like structure in which the water column at the narrowest point is disrupted.

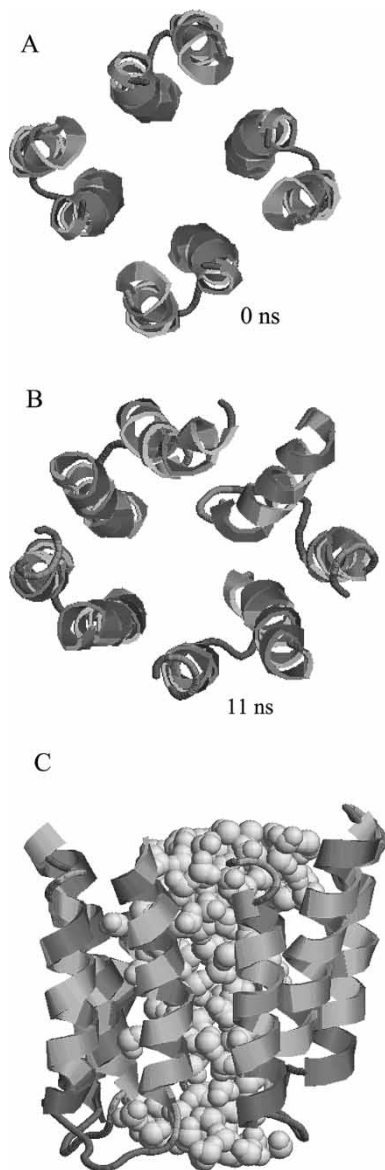


Figure 5. Tetrameric bundle of PV4 at 0 ns (A) and after 11 ns of simulations (B and C). The dark colour stands for hydrophilic residues, the grey colour for hydrophobic residues (RASMOL). The water molecules are shown in light grey and in van der Waals representation (C). Only the waters within the pore are shown. The lipid molecules and their hydrating water molecules are omitted for clarity. This figure is reproduced in colour in the online version.

Discussion

The overall approach used here draws heavily on the ‘two-’ and ‘three-stage’ models proposed by Popot and Engelman [4,5]. The model describes the principal stages of how membrane proteins are built: First the secondary structure – here the stretch of a helix – is built within the lipid membrane, then the tertiary – here the monomeric dimers – or the quaternary structure [5] (here the tetrameric bundle) is assembled. This approach has been adopted

in the literature to generate the structure of viral [11,39–41] and other channel forming proteins [42,43].

Ideal helices have been generated and used to form 2B monomers with the aim to enable an optimized packing. The tetrameric bundles are then modelled by rotating and translating the monomers in such a way that in a putative bundle their hydrophilic residues are pointing towards the lumen of the pore [24]. Each of the monomers and tetrameric bundles are subject to multi nano second MD simulations to assess their conformational stability. The orientation of the monomers within the bundle is based on the idea of hydrophilic residues forming the lumen of the pore. This is generally accepted and used so far in the literature to generate bundles from monomeric units [22,35,44–46].

The particular helical pairs have been chosen for monomers because 2B proteins from polio and coxsackie viruses have an identity of 50% and 66% for their TMDs. This makes it likely that the structures of the proteins will be similar for both species *in vivo*.

Roles of the linker region and other amino acids

An essential feature in membrane proteins is the linker or loop region which connects the TM helices within a membrane protein and is therefore involved in shaping the overall protein [46]. In the simulations all hydrophilic residues of the linker region face the aqueous medium. In the current model Arg-22 and Glu-25 interact with each other and screen the mouth of the pore whilst Asp-26 faces the intra-subunit and protein-lipid interfaces. The positions of Glu-25 and Asp-26 in this study are similar to those found for D-61 and D-62 (see [38]). The role of these amino acids in the mechanism of function of 2B of coxsackie virus has been analyzed [38]. It also has been shown that replacement of these two residues (D-61/62) leads to abrogation of multimerization and a decrease in membrane permeability. The position shown in Figure 7 suggests that Glu-25 and Asp-26 are involved in the formation of monomers, which are essential prerequisites for channel formation.

Trp-44 and Trp-46 can either face the lumen of the pore (Figure 6C) or point towards the outside of the bundle (Trp-46). They follow Pro-43 in the sequence which may lock their orientation even further. Being at the C terminus of the bundle, Trp-44 and Trp-46 are responsible for the orientation of the extra-membrane part of the C terminus. As found experimentally [38], double mutation of the conserved tryptophans located at the C-terminus

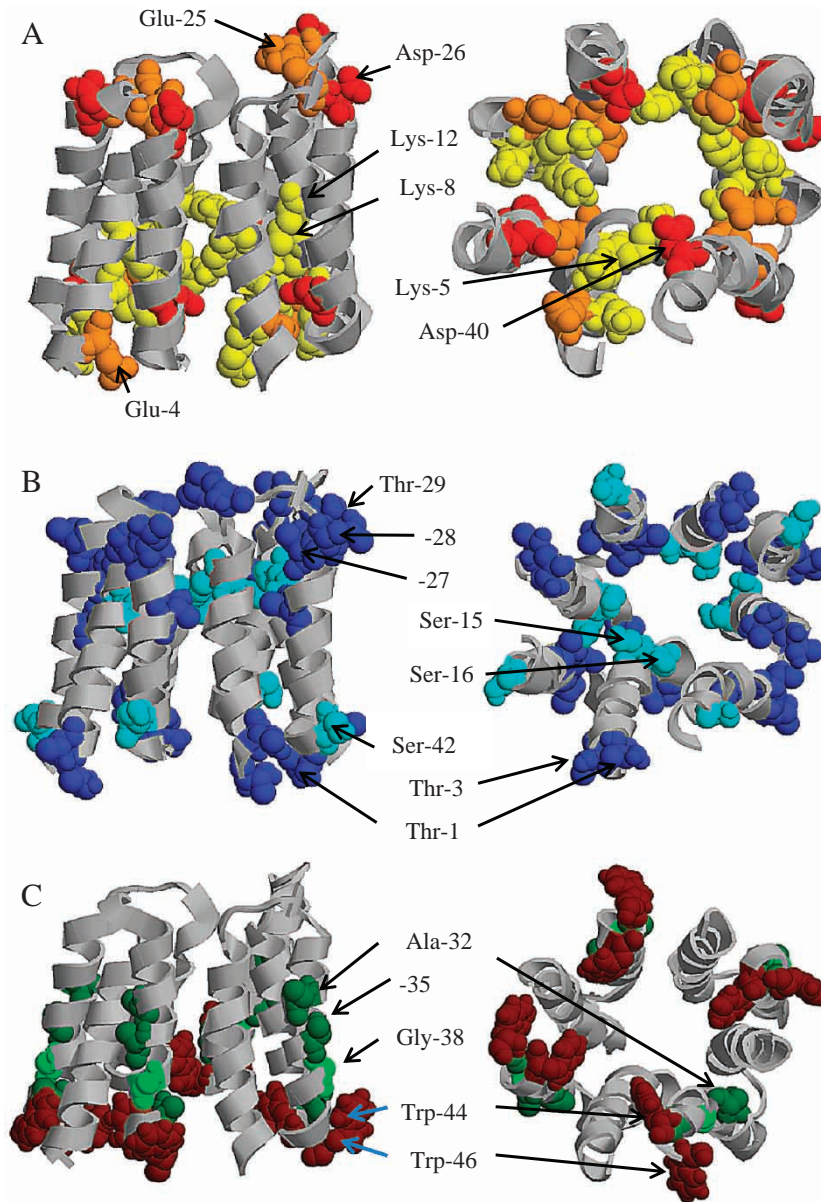


Figure 6. Models of PV4 from Figure 5 with individual amino acids are shown in their vdW representation, indicated by arrows and highlighted (RASMOL). Alanines, glycines and tryptophans are shown in panel A. The bundle is shown in a side (left column) and top view from the N and C termini (right column). Lysines, glutamic and aspartic acids are shown in panel B. Serines and threonines are shown in panel C.

of helix 2 decreases membrane permeability but does not affect the multimerization. The tryptophans, possibly together with the prolines, direct parts of the TMDs and the extra-membrane domains relevant for permeability to proper positions at the membrane surface. This further supports the idea that tryptophans are relevant for membrane protein anchoring and directing in lipid membranes. Mutations of hydrophilic residues within the short linker region between the two TMDs domains readily impair the multimerization and also decrease membrane permeability. Mutations of tryptophans towards the C terminus of the second TMD domain

show also abrogation of membrane permeability without affecting multimerization of the protein. The results are supported by similar studies on hygromycin B [38].

Lysines

The lysine residues of the amphipathic helix 1 in all monomer simulations point towards the bilayer surface (Figure 4A), with all three lysine residues having at least one water molecule within hydrogen bonding distance of $<2.2\text{\AA}$ [47]. This orientation is known as 'snorkeling' and it has been shown that the

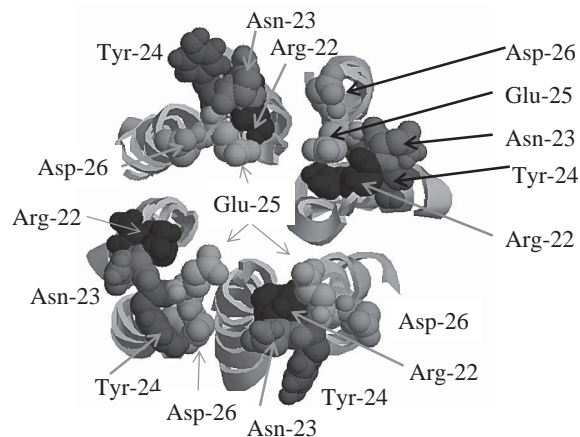


Figure 7. Tip view of the loop region with Arg-22, Asn-23, Tyr-24, Glu-25 and Asp-26 shown in vdW representation and indicated by arrows. A grey scale colour code is used (RASMOL). This figure is reproduced in colour in the online version.

energetic cost of placing a charged lysine residue into a membrane is lower if snorkeling occurs [49]. The exact position of the lysine side chain within the lipid membrane may also depend on its protonation state [50].

Tetramer

For bundle formation the helix with most of the hydrophilic residues along one side of the helix has been chosen to point towards the lumen of the tetrameric pores. This means that in the bundle, a line of three lysines followed by a serine should point towards the lumen. Such a motif has not yet been outlined on a structural level in the literature. Other hydrophilic residues such as serines and threonines in all the bundles are not forming a continuous line along one side. As for Ser-15 and Thr-1 in helix 1, they are separated by four helical turns with hydrophobic residues separating them. Part of the separation may be covered by the flexible side chains of the lysines (Lys-5, -8 and -12).

In the current most stable model, PV4, Trp-46 is at the outer side of the bundle and at a place where it will be able to fulfill its role anchoring the bundle in the lipid bilayer. Trp-44 on the other hand is facing the pore.

In the MD simulations all bundles adopt tepee-like structures, which is not unusual considering the large density of the positive charge towards the N terminus of the bundle. One may speculate whether helix 1 floats on the membrane surface rather than being inserted. This conformation may be supported by a hydrophobic line opposing the hydrophilic stretch of helix 1.

Topology

It is also suggested that interaction of helix 1 with the membrane is an essential step for assembly [29]. Therefore L-shape assembly can be envisaged, with helix 1 floating on top of the membrane and residues Thr-29, Thr-33, Asp-40 of helix 2 lining a pore. It should be mentioned that the L-shape model may also represent an ‘extreme’ orientation. Energetic investigations of whether a transition is possible under physiological conditions have not yet been undertaken. Any intermediate models, possibly involving a tepee-like structure, could also be adopted as seen in other channels [51–53].

Considering flexibility of the L shaped structure, the bundle formed could be cation selective due to Asp-40, whilst in a parallel alignment it could be anion selective due to the lysines. The bundle could even enable small molecules to traverse the pore since in parallel arrangement it adopts a tepee like structure.

PV4 is chosen as a representative bundle in the figures since it maintains finally a continuous water column throughout the simulation as a tetramer. Although a water-filled bundle may not be the ‘ultimate’ criterion for a proper structural model, the bundle represents a plausible model at the current stage of investigation.

Conclusions

A computational protocol was used to model the putative structure and assembly of the pore forming proteins from polio and coxsackie viruses. At this stage model building is based on the hypothesis that the TM motif is helical and the assembly follows the ‘two-’ and ‘three-stage’ models. On the basis of these ideas it is suggested that lysines partially contribute to the lumen of the pore. It is also concluded that this motif in combination with topological and structural flexibility may account for the experimental findings of these proteins to conduct also small molecules. This is in support of the idea of a channel/pore dualism of these proteins [54].

Acknowledgements

WBF and AW thank the Bionanotechnology IRC for financial support (GR/R45650/01). The MRC is acknowledged for grant support (MRC Programme grant G000852).

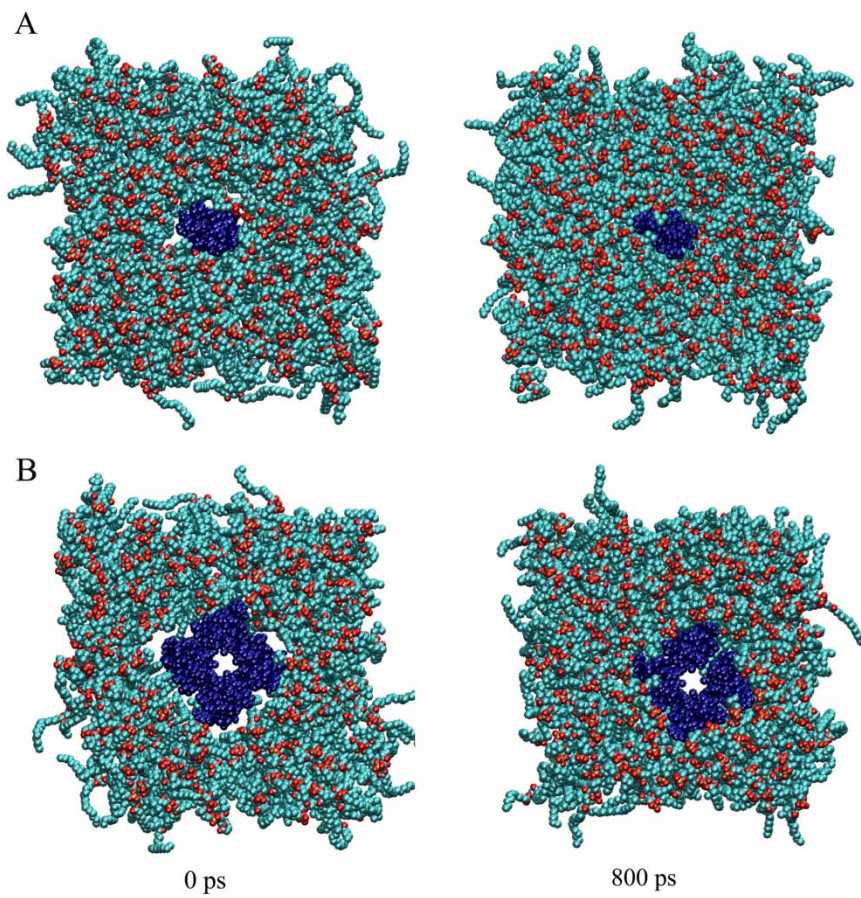
Declaration of interest: The authors report no conflicts of interest. The authors alone are responsible for the content and writing of the paper.

References

- [1] Gonzales ME, Carrasco L. 2003. Viroporins. *FEBS Lett* 552:28–34.
- [2] Fischer WB. 2005. Viral membrane proteins: Structure, function and drug design. In: Atassi MZ, editor. *Protein reviews*. Vol. 1. New York: Kluwer Academic/Plenum Publisher.
- [3] Fischer WB, Krüger J. 2009. Viral channel forming proteins. *Int Rev Cell Mol Biol* 275:35–63.
- [4] Popot J-L, Engelman DM. 1990. Membrane protein folding and oligomerization: The two-stage model. *Biochemistry* 29:4031–4037.
- [5] Engelman DM, Chen Y, Chin C-N, Curran AR, Dixon AM, Dupuy AD, Lee AS, Lehnert U, Matthews EE, Reshetnyak YK, Senes A, Popot J-L. 2003. Membrane protein folding: Beyond the two-stage model. *FEBS Lett* 555:122–125.
- [6] Bowie JU. 2005. Solving the membrane protein folding problem. *Nature* 438:581–589.
- [7] van Kuppeveld FJ, Galama JM, Zoll J, Melchers WJ. 1995. Genetic analysis of a hydrophobic domain of coxsackie B3 virus protein 2B: A moderate degree of hydrophobicity is required for a cis-acting function in viral RNA synthesis. *J Virol* 69:7782–7790.
- [8] Aldabe R, Barco A, Carrasco L. 1996. Membrane permeabilization by poliovirus proteins 2B and 2BC. *J Biol Chem* 271:23134–23137.
- [9] van Kuppeveld FJM, Melchers WJG, Kirkegaard K, Doedens JR. 1997. Structure-function analysis of coxsackie B3 virus protein 2B. *Virology* 227:111–118.
- [10] Carrère-Kremer S, Montpellier-Pala C, Cocquerel L, Wychowski C, Penin F, Dubuisson J. 2002. Subcellular localization and topology of the p7 polypeptide of Hepatitis C virus. *J Virol* 76:3720–3730.
- [11] Patargias G, Zitzmann N, Dwek R, Fischer WB. 2006. Protein-protein interactions: Modeling the hepatitis C virus ion channel p7. *J Med Chem* 49:648–655.
- [12] Lu W, Zheng B-J, Xu K, Schwarz W, Du L, Wong CKL, Chen J, Duan S, Deubel V, Sun B. 2006. Severe acute respiratory syndrome-associated coronavirus 3a protein forms an ion channel and modulates virus release. *Proc Natl Acad Sci USA* 103:12540–12545.
- [13] von Heijne. 1992. Membrane protein structure prediction. Hydrophobicity analysis and the positive inside rule. *J Mol Biol* 225:487–494.
- [14] Adams PD, Arkin IT, Engelman DM, Brünger AT. 1995. Computational searching and mutagenesis suggest a structure for the pentameric transmembrane domain of phospholamban. *Nature Struct Biol* 2:154–162.
- [15] Adams PD, Engelman DM, Brünger AT, Sansom MSP. 1996. Improved prediction for the structure of the dimeric transmembrane domain of glycophorin A obtained through global searching. *Proteins* 26:257–261.
- [16] Forrest LR, Kukol A, Arkin IT, Tieleman DP, Sansom MS. 2000. Exploring models of the influenza A M2 channel: MD simulations in a phospholipid bilayer. *Biophys J* 78:55–69.
- [17] Cordes F, Kukol A, Forrest LR, Arkin IT, Sansom MSP, Fischer WB. 2001. The structure of the HIV-1 Vpu ion channel: Modelling and simulation studies. *Biochim Biophys Acta* 1512:291–298.
- [18] Kim S, Chamberlain AK, Bowie JU. 2003. A simple method for modeling transmembrane helix oligomers. *J Mol Biol* 329:831–840.
- [19] Vereshaga YA, Volynsky PE, Pustovalova JE, Nolde DE, Arseniev AS, Efremov RG. 2007. Specificity of helix packing in transmembrane dimer of the cell death factor BNIP3: A molecular modeling study. *Proteins: Struct Func Gen* 69:309–325.
- [20] Psachoulia E, Fowler PW, Bond PJ, Sansom MSP. 2008. Helix-helix interactions in membrane proteins: Coarse-grained simulations of glycophorin A helix dimerization. *Biochemistry* 47:10503–10512.
- [21] Krüger J, Fischer WB. 2008. Exploring the conformational space of Vpu from HIV-1: A versatile and adaptable protein. *J Comp Chem* 29:2416–2424.
- [22] de Jong AS, Wessels E, Dijkman HBPM, Galama JMD, Melchers WJG, Willems PHGM, van Kuppeveld FJM. 2003. Determinants for membrane association and permeabilization of the coxsackie virus 2B protein and the identification of the Golgi complex as the target organelle. *J Biol Chem* 278:1012–1021.
- [23] Nieva JL, Agirre A, Nir S, Carrasco L. 2003. Mechanism of membrane permeabilization by picornavirus 2B viroporin. *FEBS Lett* 552:68–73.
- [24] de Jong AS, Visch H-J, de Mattia F, van Dommelen MM, Swart HG, Luyten T, Callewaert G, Melchers WJ, Willems PH, Van Kuppeveld FJ. 2006. The coxsackie virus 2B protein increases efflux of ions from the endoplasmic reticulum and Golgi, thereby inhibiting protein trafficking through the Golgi. *J Biol Chem* 281:14144–14150.
- [25] Cuconati A, Xiang W, Lahser F, Pfister T, Wimmer E. 1998. A protein linkage map of the P2 nonstructural proteins of poliovirus. *J Virol* 72:1297–1307.
- [26] de Jong AS, Schrama IW, Willems PH, Galama JM, Melchers WJ, van Kuppeveld FJ. 2002. Multimerization reactions of coxsackie virus proteins 2B, 2C and 2BC: A mammalian two-hybrid analysis. *J Gen Virol* 83:783–793.
- [27] van Kuppeveld FJM, Melchers WJG, Willems PHGM, Gadella TWJ Jr. 2002. Homomultimerization of the coxsackie virus 2B protein in living cells visualized by fluorescence resonance energy transfer microscopy. *J Virol* 76:9446–9456.
- [28] Agirre A, Barco A, Carrasco L, Nieva JL. 2002. Viroporin-mediated membrane permeabilization. Pore formation by nanostructural poliovirus 2B protein. *J Biol Chem* 277:40434–40441.
- [29] van Kuppeveld FJM, Galama JMD, Zoll J, van den Hurk PJJ, Melchers WJG. 1996. Coxsackie B3 virus protein 2B contains a cationic amphipathic helix that is required for viral RNA replication. *J Virol* 70:3876–3886.
- [30] Brünger AT. 1992. X-PLOR Version 3.1. A system for X-ray crystallography and NMR. New Haven, CT: Yale University Press.
- [31] Brünger A, Adams P, Clore G, Gros W, Grosse-Kunstleve R, Jiang J, Kuszewski J, Nilges M, Pannu N, Read R, Rice L, Simonson T, Warren G. 1998. Crystallography and NMR system: A new software suite for macromolecular structure determination. *Acta Crystallogr D Biol Crystallogr* 54:905–921.
- [32] Xiang Z, Soto CS, Honig B. 2002. Evaluating conformational free energies: The colony energy and its application to the problem of loop prediction. *Proc Natl Acad Sci USA* 99:7432–7437.
- [33] Candler A, Featherstone M, Ali R, Maloney L, Watts A, Fischer WB. 2005. Computational analysis of mutants in the transmembrane region of Vpu from HIV-1. *Biochim Biophys Acta* 1716:1–10.
- [34] Lemaitre V, Ali R, Kim CG, Watts A, Fischer WB. 2004. Interaction of amiloride and one of its derivative with Vpu from HIV-1: A molecular dynamics simulation. *FEBS Lett* 563:75–81.

- [35] Lee B, Richards FM. 1971. The interpretation of protein structures: Estimation of static accessibility. *J Mol Biol* 55:379–400.
- [36] Mitaku S, Hirokawa T, Tsuji T. 2002. Amphiphilicity index of polar amino acids as an aid in the characterization of amino acid preference at membrane-water interfaces. *Bioinformatics* 18:608–616.
- [37] de Jong AS, Melchers WJ, Glaudemans DH, Willems PH, van Kuppeveld FJ. 2004. Mutational analysis of different regions in the coxsackie virus 2B protein: Requirements for homo-multimerization, membrane permeabilization, subcellular localization, and virus replication. *J Biol Chem* 279:19924–19935.
- [38] Kukol A, Arkin IT. 1999. Vpu transmembrane peptide structure obtained by site-specific fourier transform infrared dichroism and global molecular dynamics searching. *Biophys J* 77:1594–1601.
- [39] Zhong Q, News DM, Pattnaik P, Lear JD, Klein ML. 2000. Two possible conducting states of the influenza A virus M2 ion channel. *FEBS Lett* 473:195–198.
- [40] Cordes FS, Tustian A, Sansom MSP, Watts A, Fischer WB. 2002. Bundles consisting of extended transmembrane segments of Vpu from HIV-1: Computer simulations and conductance measurements. *Biochemistry* 41:7359–7365.
- [41] Dieckmann GR, Lear JD, Zhong Q, Klein ML, DeGrado WF, Sharp KA. 1999. Exploration of the structural features defining the conduction properties of a synthetic ion channel. *Biophys J* 76:618–630.
- [42] Davies LA, Klein ML, Scharf D. 1999. Molecular dynamics simulation of a synthetic four- α -helix bundle that binds the anesthetic halothane. *FEBS Lett* 455:332–338.
- [43] Grice AL, Kerr ID, Sansom MSP. 1997. Ion channels formed by HIV-1 Vpu: A modelling and simulation study. *FEBS Lett* 405:299–304.
- [44] Fischer WB, Pitkeathly M, Wallace BA, Forrest LR, Smith GR, Sansom MSP. 2000. Transmembrane peptide NB of influenza B: A simulation, structure, and conductance study. *Biochemistry* 39:12708–12716.
- [45] Lopez CF, Montal M, Blasie JK, Klein ML, Moore PB. 2002. Molecular dynamics investigation of membrane-bound bundles of the channel-forming transmembrane domain of viral protein U from the Human Immunodeficiency Virus HIV-1. *Biophys J* 83:1259–1267.
- [46] Tastan O, Klein-Seetharaman J, Meirovitch H. 2009. The effect of loops on the structural organization of α -helical membrane proteins. *Biophys J* 96:2299–2312.
- [47] Steiner T. 2002. The hydrogen bond in the solid state. *Angew Chem Int Ed* 41:49–76.
- [48] Strandberg E, Killian JA. 2003. Snorkeling of lysine side chains in transmembrane helices: How easy can it get? *FEBS Lett* 544.
- [49] Tayefeh S, Kloss T, Thiel G, Hertel B, Moroni A, Kast SM. 2007. Molecular dynamics simulation study of the cytosolic mouth in Kcv-type potassium channels. *Biochemistry* 46:4826–4839.
- [50] Doyle DA, Cabral JM, Pfuetzner RA, Kuo A, Gulbis JM, Cohen SL, Chait BT, MacKinnon R. 1998. The structure of the potassium channel: molecular basis of K^+ conduction and selectivity. *Science* 280:69–77.
- [51] Sukharev S, Betanzos M, Chiang C-S, Guy HR. 2001. The gating mechanism of the large mechanosensitive channel MscL. *Nature* 409:720–724.
- [52] Wang W, Black SS, Edwards MD, Miller S, Morrison EL, Bartlett W, Dong C, Naismith JH, Booth IR. 2008. The structure of an open form of an *E. coli* mechanosensitive channel at 3.45 Å resolution. *Science* 321:1179–1183.
- [53] Mehnert T, Routh A, Judge PJ, Lam YH, Fischer D, Watts A, Fischer WB. 2008. Biophysical characterisation of Vpu from HIV-1 suggests a channel-pore dualism. *Proteins* 70:1488–1497.

This paper was first published online on iFirst on 21 August 2009.



Supplementary Figure. The simulation box of PV4 monomer (helix 1 and 2) (A) and tetramer (B) is shown at the beginning (left) and end (right) of an 800 ps equilibration run. The protein is shown in black, lipids in light grey with their oxygen atoms shown in darker grey. After 800 ps equilibration the protein is packed within the lipid membrane.